Journal of Information Systems Engineering and Management
2025, 10(16s)
e-ISSN: 2468-4376
https://www.jisem-journal.com/

Research Article

Estimation of Global Solar Radiation in the Eastern Upland Region of Taplejung, Nepal, using RadEst 3.0 Software

Basanta Kumar Rajbanshi[1], Ram Gopal Singh[2], Kishor Khatiwada[3], Anil Thapa[3] Binod Kharel[4] Bed Raj KC[5]

[1]Research Scholar, Shri Ramswaroop Memorial University (SRMU), Devaroad-Lucknow, Barabanki, India
basantaraz22@gmail.com, basantaraz05@gmail.com
ORCID ID: 0009-0003-7953-7475
[2]Dean, Faculty of Physical Sciences, Shri Ramswaroop Memorial University (SRMU), Devaroad-Lucknow, Barabanki, India
dean.phy@srmu.ac.in
[3]Research Scholar, St. Xavier's College, Tribhuvan University, Kathmandu, Nepal cherthapa@gmail.com kishorkhatiwadasxc@gmail.com
[4]Research Scholar, Patan Multiple Campus, Tribhuvan University, Kathmandu, Nepal binodkharel2046@gmail.com
[5]Vice Chancellor, Pokhara University, Gandaki Province, Nepal bedrajkc@yahoo.com

ARTICLE INFO

Received: 03 Dec 2024

Revised: 26 Jan 2025

Accepted: 08 Feb 2025

ABSTRACT

Understanding solar radiation distribution in each geographic region is essential for developing solar energy technology. This research estimates daily global solar radiation (GSR) at Eastern Upland, Taplejung, Nepal (27.35° N, 87.69° E, 2840 m) using RadEst 3.0. It incorporates seven meteorological parameters: rainfall, maximum and minimum temperatures, solar radiation, maximum and minimum humidity, and average wind speed, for 2020, 2021, and 2023. Four different models, Donatelli and Bellocchi (DB), Campbell and Donatelli (CD), Bristow and Campbell (BC), and Donatelli-Campbell-Bristow-Bellocchi (DCBB), are used for calculating radiation. In evaluating the models' performance, we utilized various statistical methods, such as coefficient of determination (R2), mean bias error (MBE), mean percentage error (MPE), correlation coefficient (r), root mean square error (RMSE), and mean error (ME). Parameter fitting (PF) calibrates all four models by maximizing R2, minimizing CRM, and RMSE. In 2020, 2021, and 2023, the annual mean GSR values were 15.0 ± 0.31 MJ/m2/day, 14.6 ± 0.28 MJ/m2/day, and 15.9 ± 0.31 MJ/m2/day, respectively. The maximum GSR values recorded in 2020, 2021, and 2023 were 29.2 MJ/m2/day, 32.0 MJ/m2/day, and 30.0 MJ/m2/day, respectively. Similarly, R2 was found to be 0.64, 0.64, and 0.65 in 2020, 2021, and 2023 respectively in the CD model for the three years which are larger than all other models. The CD model offers the most accurate global solar radiation (GSR) estimates in this area. This article recommends implementing a comprehensive program to promote and require using renewable energy resources (RES), especially solar energy, across eastern Nepal.

Keywords: RadEst 3.0 program, air transmissivity, atmospheric variables, pyranometer, and global solar radiation

1. INTRODUCTION

Nepal has diverse topography, with mountains of varying heights, shaping its geomorphology. On the global map, Nepal is in the solar energy-friendly range. (Team et al. 2012) Its expanded area is 147,516 square km, approximately 800 km long and 200 km wide. It is located between longitude 80°4'- 88°12' E and latitude 26°22' - 30°27' N. It shares borders with China and India and is a landlocked nation. Nepal is a unique region with a diverse climate and biodiversity because its climate changes every 200 m above sea level. It lacks access to its fossil fuel supplies, such as coal, oil, or gas reserves. A shortage in energy supply is the reason for Nepal's economic and social underdevelopment.

According to the Solar and Wind Energy Resource Assessment (SWERA) by the Alternative Energy Promotion Centre (AEPC), Nepal has an economic potential for on-grid solar PV installations of up to 2,100 MW. There are now 974,000 residential solar PV systems built as of 2022; mainly concentrated in remote districts of Western Nepal where access to grid electricity is limited. (WECS, Energy Synopsis Report, 2023)

2.2%, 27.8%, and 70% of the total energy consumed in the 2017/18 fiscal year came from renewable, traditional, and commercial sources respectively. Among traditional energy sources, firewood is the most common. Its use is wasteful and causes the loss of forests. In addition, there is a health risk associated with indoor air pollution from open fireplaces. According to Lamsal, 22% of people do not have access to power, primarily provided in urban areas. During the dry season, when power cut-off occurs for many hours daily, businesses, industries, and individual households suffer greatly from the lack of power. The commercial and industrial sectors, as well as the general public and private households, are not aware of the environmental and financial benefits of energy efficiency. The standardization of energy-efficient home products, lighting, and industrial advancements is currently lacking.

Fuel sales increased in 2021 by 10.87%, diesel by 12.6%, kerosene by 21.61%, and LPG by 6.19%. On the other hand, Alternative Technology Fuels (ATF) sales dropped considerably by 65.32%. Petrol sales increased by 40.43% in 2022, almost quadrupling in value. Likewise, there was a 32.24%, 11.5%, and 74.55% growth in the sales values of diesel, LPG, and ATF, respectively. Kerosene sales, however, decreased by 4.99%. (WECS, Energy Synopsis Report, 2023)

Solar radiation is a secure and clean energy source. The average solar insolation in the nation ranges from 3.6 to 6.2 kWh/m^2/day per year. According to Shrestha et al. (2003), Nepal has 300 sunny days and 6.8 hours of sunshine each year, indicating a large potential for free and clean solar energy. The current yearly mean GSR is 4.23 kWh/m^2/day, according to Poudyal (2015). Therefore, in developing Asian nations like Nepal, solar energy is a pivotal solution to our global energy challenges. (Joshi et. al.2020)

Several formulae of different difficulty levels and the typical work of Angstrom may be used to easily calculate the GSR from the recorded sunlight hour and other meteorological information. (Angstrom 1924; Iqbal 1983). The solar energy potential of Shenzhen, China, was estimated by An Y. et al. using GIS-based urban residential environmental data. (Yaning An et al. 2023). Romero-Ramos, J.A. used a GIS-AHP approach to investigate at the possibilities of using solar power to meet the thermal consumption in the industrial sector of southeast Spain. (Romero-Ramos, J.A. et al., 2023).

To figure out the GSR for northwest Nigeria, Olomiyesan et al. analyzed the effectiveness of four methods. These four methods were compared with three existing methods (Garika, Hargreaves, and Samani) using monthly meteorological information on temperature, sunlight hour, and GSR. (Olomiyesan et al., 2017) Based on Ethiopia's solar hours and temperature, Nage reviews many models. (Nage 2018). Haushan Li et al. suggested an innovative model for the computation of GSR in 65 areas in China, depending on the Hargreaves and Samani (HS) technique. (Li et al. 2014) The newly established model is compared by the authors with the Chen, Samani and HS models. Akpootu D. O. et. al. calculated global solar radiation in Maiduguri, Nigeria using sunshine and temperature-based models. (Akpootu D. O. et. al. 2023)

Hassan et al. calculated the capabilities of twenty different models that use air temperature to make predictions. Seventeen of these models were newly developed. The other three models used for estimating GSR specifically in Egypt were previously developed by Allen in 1997, Goodin et al. in 1999, and Annandale et al. in 2002. (Hassan et al. 2016). K A Narejo et al. created new mathematical formulas for estimating solar radiation in Pakistan based on existing standards. Using these new formulas, they calculated three types of solar radiation - global, beam, and diffuse - for five cities around the world (New York, Tokyo, Karachi, Sydney, and London). (K A Narejo et al. 2024) González-Plaza E et al. developed a model to predict monthly global solar radiation in Spain. This model uses artificial intelligence, temperature measurements, and geographical information. (González-Plaza, E et al. 2024). Joshi et al. used various established methods to calculate the amount of GSR received in Khumaltar, Nepal. (Joshi et al. 2021). Rajbanshi et al. used the RadEst 3.0 program to estimate the daily global solar radiation (GSR) in Biratnagar, a lowland city in eastern Nepal. (Rajbanshi et al. 2024B) Dhakal et al. explored various methods, including traditional mathematical formulas, and advanced computer learning techniques, to predict the amount of GSR in Biratnagar, Nepal. These methods depend on temperature data. (Dhakal et al. 2020). Joshi et al. used a specialized computer program called RadEst 3.0 to calculate the daily amount of GSR received in Simikot, located in the western highlands of Nepal. (Joshi et al. 2022). In contrast, Rajbanshi et al. applied the same program to calculate the daily GSR in Dhankuta, a hilly region in eastern Nepal. (Rajbanshi et al. 2024A)

Bristow and Campbell originate the diurnal variations in near-surface air temperature and radiation transmissivity through the atmosphere. This model has been refined over the previous few years and has been utilized in many

investigations. A correction component that took into account the effects of seasonality in the mid-latitude region was added to the models. The weather generators were designed using this idea. (Bristow and Campbell 1984)

Donatelli and Bellocchi focused on enhancing the methods used to track seasonal changes in solar radiation at different locations. (Donatelli and Bellocchi 2001) (Donatelli et al. 2003). Using the RadEst 3.0 programme, Poudyal et al. calculated the GSR in Kathmandu, Nepal during the years 2005 and 2007 (Poudyal et al. 2013). Similarly, at Simara Airport in Nepal, they calculated the global solar radiation (Poudyal et al. 2012). Based on data from the years 2011 and 2013, Chhetri and Gurung in Jumla, Nepal, calculated the GSR using the RadEst 3.00 programme (Chhetri and Gurung 2017).

This research aims to analyze the distribution of solar energy in Nepal, where there is a lot of untapped solar potential. The study uses local weather data and sophisticated modeling techniques to accurately determine global solar radiation levels. By comparing different models, the researchers find the best method for estimating solar radiation in Taplejung. This study provides valuable information that can be used for planning future solar energy projects and promoting sustainable energy development in Nepal.

2. RADEST 3.0 PROGRAM

Determining the global solar radiation of a region requires high-quality data from extensive radiation observations across all major climatic zones. Various empirical formulas have been developed to calculate the daily GSR at various locations across the globe, utilizing different parameters. A possible option that uses the highest and lowest temperatures to calculate the daily GSR is the RadEst 3.0 software.

This paper presents the RadEst 3.0 software, which enables the user to calculate the daily GSR using the average speed of the air, precipitation, maximum and minimum humidity, highest and lowest temperature, and geographic location. The main aim of this research work is to determine the best model for the relationship between GSR, temperature, and precipitation to facilitate future research in similar geographical areas and to support the advancement of solar power technology in Nepal. Because air temperature, humidity, wind speed, and precipitation are readily available from meteorological stations worldwide, RadEst 3.0 software was chosen due to its reliability, user-friendliness, and versatility.

A joint project between the FAO-SDRN-Agrometeorology Group and ISCI-Crop Science led to the creation of the RadEst 3.00 software. This program employs four basic models to estimate daily global solar radiation at a specific location. The results generated by the software can be analyzed using statistical and visual techniques.

Models

Four models estimate daily solar radiation reaching the Earth's surface. These models are named DCBB, BC, CD, and DB, developed by Donatelli, Campbell, Bristow, and Bellocchi. These models employ statistical methods to calculate estimated radiation based on several input factors. These factors include:

tt_i = estimated atmospheric transmissivity,

τ = clear sky transmissivity,

ΔT = average monthly temperature

T_{max} = maximum daily air temperature

T_{min} = minimum daily air temperature,

b = temperature range coefficient

c = highly sensitive empirical parameter,

T_{nc} = thermal factor

c_1 = magnitude parameter for seasonal variation

c_2 = profile coefficient for seasonal variation

i = day number of the year, i = 1 to 365 or 366

$f(T_{avg})$ = average temperature function,

$f(T_{min})$ = minimum temperature function

Est Rad_i = estimated radiation (MJ m^{-2} day^{-1})

$PotRad_i$ = Extraterrestrial radiation i.e. radiation beyond Earth's atmosphere (MJ m^{-2} day^{-1})

These models determine how much solar radiation passes through the atmosphere by analyzing daily temperature fluctuations. The predicted amount of solar radiation (Est Radi) reaching the Earth's surface is calculated by multiplying the estimated atmospheric transmissivity (tti) by the total potential solar radiation (Pot Radi) at the top of the atmosphere.

Est Rad_i = tt_i Pot Rad_i

$$Pot\ Red_{doy} = 117.5 dd_2 \frac{h_s Sin(lat)\ Sin(dec) + Cos(lat)\ Sin(h_s)}{\pi} \quad (1)$$

This equation utilizes the following variables: latitude of the observation point (lat) in degrees, solar declination (dec), the sun's distance (dd2), and half-day duration (hs).

2.1 Bristow and Campbell Model

The initial model, developed by Bristow and Campbell, served as a foundation for subsequent models. This model calculates the daily amount of incoming solar radiation by examining the connection between daily temperature fluctuations and overall solar radiation. It assumes that higher daily temperatures correspond to clearer skies (lower transmissivity) and vice versa.

Cloud cover impacts both maximum and minimum temperatures. Cloudy conditions lead to warmer nighttime temperatures due to heat trapped by clouds, while clear skies result in colder nights because heat escapes more readily. Conversely, clear skies cause higher daytime temperatures due to increased solar radiation reaching the Earth's surface. This method of estimating solar radiation based on temperature differences has been widely applied and refined over the years.

Estimated atmospheric transmissivity is

$$tt_i = \tau \left[1 - exp\left(\frac{-b\ \Delta T_i^C}{month\ \Delta T}\right)\right] \quad (2)$$

Hence from the equation, estimated radiation provided is given by,

$$Est\ Red_i = \tau \left[1 - exp\left(\frac{-b\ \Delta T_i^C}{month\ \Delta T}\right)\right] PotRed_i \quad (3)$$

Where,

$$\Delta T_i = T_{max_i} - \frac{T_{min_i} + T_{min(i+j)}}{2} \quad (4)$$

2.2 Campbell and Donatelli Model

The Campbell and Donatelli (CD) model was developed by refining the original Bristow and Campbell (BC) model. To account for seasonal changes common in mid-latitude regions like Nepal, the CD model incorporates a correction factor. This factor, known as T_{nc}, adjusts the estimated transmissivity, particularly during summer nights. The model calculates transmissivity as,

$$tt_i = \tau\left[1 - exp\left\{-b \times f\left(T_{avg}\right) \Delta T_i^2\ f(T_{min})\right\}\right] \quad (5)$$

Thus,

Est Red_i = $\tau\left[1 - exp\left\{-b \times f\left(T_{avg}\right) \Delta T_i^2\ f_1(T_{min})\ PotRed_i\right\}\right]$ (6)

Where,

$$T_{avg} = \frac{T_{max_i} + T_{min_i}}{2} \quad (7)$$

2.3 Donatelli and Bellocchi Model

The third model, developed by Donatelli and Bellocchi, estimates total solar energy based on air temperature. Unlike previous models, this one considers changes in atmospheric clarity throughout the year. To account for seasonal variations, the model uses additional factors, c_1 and c_2, to calculate temperature differences. The model determines transmissivity as,

$$tt_i = \tau\left[1 + f(i)\left[1 - exp\left\{\frac{-b\,\Delta T^2}{\Delta T_{week}}\right\}\right]\right] \quad (8)$$

Providing radiation estimates as,

$$\text{EstRed}_i = \tau\left[1 + f(i)\left[1 - exp\left\{\frac{-b\,\Delta T_i^2}{\Delta T_{week}}\right\}\right]\right] PotRed_{\,i} \quad (9)$$

Where,

$$f(i) = c_1\left[sin\left(i\,c_2\frac{\pi}{180}\right) + cos\left\{i\,f(c_2)\frac{\pi}{180}\right\}\right] \quad (10)$$

$$f(c_2) = 1\text{–}1.90\,c_3 + 3.83c_3^2 \quad (11)$$

$$c_3 = c_2 \text{ integer } (c_2) \quad (12)$$

2.4 Donatelli-Campbell-Bristow-Bellocchi Model

The fourth model trusts on atmospheric air condition changes. All three models offer customizable features i.e. can be turned on and off. For example, the model can be simplified by setting parameter c_1 to zero. Under specific conditions, where the T_{nc} factor is excluded and average monthly temperature differences are used, the BC model becomes equivalent to the DCBB model. The estimated transmissivity under these circumstances is,

$$tt_i = \tau\left[1 + f(i)\left[1 - exp\left\{\frac{-b\,\Delta T^2 f(T_{min})}{\Delta T_{avg}}\right\}\right]\right] \quad (13)$$

Which provides radiation estimates as,

$\text{EstRed}_i =$

$$\tau\left[1 + f(i)\left[1 - exp\left\{\frac{-b\,\Delta T_i^2 f(T_{min})}{\Delta T_{avg}}\right\}\right]\right] PotRed_{\,i} \quad (14)$$

Where,

$$f(i) = c_1\left[sin\left(i\,c_2\frac{\pi}{180}\right) + cos\left\{i\,f(c_2)\frac{\pi}{180}\right\}\right] \quad (15)$$

$$f(c_2) = 1\text{–}1.90\,c_3 + 3.83c_3^2 \quad (16)$$

$$f(T_{avg}) = 0.017exp\left\{\,exp\left(-0.053 \times T_{avg}\right)\right\} \quad (17)$$

Where,

$$T_{avg} = \frac{T_{max_i} + T_{min_i}}{2} \quad (18)$$

$$f(T_{min}) = exp\frac{T_{min}}{T_{nc}} \quad (19)$$

$c_3 = c_2$ integer (c_2)

3 TECHNIQUES AND INSTRUMENTATION

3.1 Study Site Determination

Based on geography, Taplejung is a Himalayan area near the third-highest peak in the world, Kanchenjunga (8586 m). The study site is located at an elevation of 2840 meters above sea level. It is located at Lat. 27.35 N and Lon. 87.69 E. Taplejung is Nepal's third-largest district, spanning 3,646 km². It lies in Koshi province. The district shares borders with Tehrathum and Panchthar District in the south, Sankhuwasabha District in the west, Tibet, China to the north and Sikkim, India to the east.

The average temperature in Taplejung varies. It generally has a moderate climate, with warmer summer temperatures and colder winter temperatures. In winter, temperatures can drop to between 0°C and 10°C, while in spring, they can rise to between 10°C and 20°C. In the summer, the temperature can reach up to 25°C, making it quite warm. Autumn brings a return to cooler temperatures, with peaks of 10°C to 20°C.

3.2 Instrument

The Department of Hydrology and Meteorology of the Government of Nepal (DHM/GoN) supplied meteorological data for Taplejung covering the years 2020, 2021, and 2023. This data, encompassing solar radiation, highest and lowest temperatures, precipitation, humidity levels, and wind speed, served as input for the models. A maximum-minimum thermometer is used to measure temperature, and a Udometer is used to measure rainfall. Pyranometer CMP6 is used to test GSR. A thermocouple provides the foundation for this device. It reads directly into the data recorder as radiation intensity in w/m^2. It transforms radiation directly into a temperature differential, which appears as a voltage difference. This device is capable of detecting light across a broad spectrum from 310 to 2800 nanometers and can function in temperatures ranging from -40 to 80 degrees Celsius.

3.3 File Structure

The input data is stored in a plain text (ASCII) format without column headings. Each DAT file (compatible with Golden Software Surfer 2019) contains eight space-separated columns of yearly model data (days 1 to 365 or 366 for leap year). These columns represent rainfall (millimetres), maximum and minimum temperature (degrees Celsius), global solar radiation (megajoules per square meter per day), maximum and minimum humidity (percentage), and wind speed (meters per second). Using input data from Taplejung, Nepal, the daily values of GSR have been calculated for 2020, 2021, and 2023.

3.4 Input Structure

The RadEst ver. 3.00 software requires the input of latitude, longitude, and altitude for the desired location. Clear sky transmissivity values should be set within the range of 0.6 to 0.8. Latitude is utilized in the computation of estimated radiation, and clear sky transmissivity is employed to calculate the atmospheric transmissivity coefficient.

3.5 Analysis

The location, including latitude, longitude, and altitude, should be introduced initially. Subsequently, the file is to be opened in the American Standard Code for Information Interchange (ASCII) format. Automatic optimization (AO) and parameter fitting (PF) techniques are applied in various models. For comparison and GSR estimation, a minimum of two years of data are needed. The accuracy of AO is lower than that of PF. To align estimated radiation with measured values, the parameter fitting process was adjusted to achieve equivalent averages. A graphical comparison between estimated and measured radiation was conducted. Statistical metrics, including mean bias error (MBE), correlation coefficient (r), coefficient of determination (R^2), root mean square error (RMSE), mean percentage error (MPE), mean error (ME), and coefficient of variation (CV), were generated by the models to evaluate the accuracy of the estimations. To support the models, several tools are used.

4 RESULTS AND DISCUSSION

Every model undergoes auto-optimization testing, and the estimated GSR that is produced significantly differs from the measured GSR. The four models were calibrated using parameter fitting (PF) based on 2023 Taplejung data by maximizing the R^2 while minimizing the RMSE and CRM. Table 1 presents a comparison of measured and model-estimated average, maximum, and annual total GSR values for both auto-optimization and parameter fitting in 2023 for Taplejung. The average annual GSR was determined to be 15.9 MJ/m^2/day. Compared to other models, the CD model has a value that is almost exactly closer. The CD model outperformed other models in estimating the total GSR for 2023. The measured total solar radiation of 5799 MJ/m^2 closely aligns with the CD model's PF fitting value of 5743 MJ/m^2/day, indicating its superior accuracy in GSR estimation for 2023.

The GSR of the years 2020 and 2021 is estimated by using the calibrated parameter values from the year 2023. The measured and estimated GSR values were found to be very similar. Tables 2 and 3 present the parameter fitting-based test results for 2020 and 2021. The CD model exhibited performance comparable to the other three models in terms of maximum, average, and annual total GSR values across all three years (2020, 2021, and 2023). Consequently, the CD model is considered superior for estimating GSR in high-altitude regions during these years.

Table 1 Measured and modeled GSR metrics for Taplejung in 2023, including average, maximum, and annual totals.

Model	Average GSR (MJ/m²/day)			Maximum GSR (MJ/m²/day)			Total GSR (MJ/m²)		
	AO	Mea	PF	AO	Mea	PF	AO	Mea	PF
BC	15.6	15.9	15.9	25.8	30.0	26.0	5701	5799	5787
CD	15.7	15.9	15.9	25.6	30.0	25.8	5743	5799	5816
DB	15.4	15.9	15.9	24.4	30.0	24.7	5631	5799	5786
DCBB	15.2	15.9	15.9	24.0	30.0	24.2	5530	5799	5795

Table 2 Measured and modeled GSR metrics for Taplejung in 2021, including average, maximum, and annual totals.

Model	Average GSR (MJ/m²/day)			Maximum GSR (MJ/m²/day)			Total GSR (MJ/m²)		
	AO	Mea	PF	AO	Mea	PF	AO	Mea	PF
BC	14.5	14.6	14.9	23.6	32.0	24.0	5281	5319	5431
CD	14.5	14.6	14.8	24.6	32.0	24.8	5306	5319	5408
DB	14.3	14.6	14.9	23.1	32.0	23.0	5226	5319	5441
DCBB	13.9	14.6	14.5	21.3	32.0	22.5	5056	5319	5309

Table 3 Measured and modeled GSR metrics for Taplejung in 2020, including average, maximum, and annual totals.

Model	Average GSR (MJ/m²/day)			Maximum GSR (MJ/m²/day)			Total GSR (MJ/m²)		
	AO	Mea	PF	AO	Mea	PF	AO	Mea	PF
BC	14.7	15.0	15.0	24.4	29.2	24.7	5351	5472	5457
CD	14.8	15.0	14.6	24.5	29.2	24.3	5406	5472	5337
DB	14.6	15.0	15.0	23.7	29.2	24.7	5319	5472	5467
DCBB	14.3	15.0	14.7	23.8	29.2	24.2	5205	5472	5380

Figure 6 illustrates how GSR changes throughout the seasons of 2023, 2021, and 2020. The maximum GSR occurs in Spring (18.13 ± 0.57 MJ/m²/day, 16.97 ± 0.64 MJ/m²/day, and 18.72 ± 0.70 MJ/m²/day for the years 2020, 2021, and 2023 respectively) due to the clear weather after the monsoon. The lowest GSR value is found in winter (12.40 ± 0.53 MJ/m²/day, 12.43 ± 0.36 MJ/m²/day, and 13.65 ± 0.33 MJ/m²/day for years 2020, 2021, and 2023 respectively) due to cloud cover sky and rainfall.

Solar radiation levels were highest during spring and lowest during winter in all three years. Springtime solar radiation exceeded that of summer and autumn, likely due to lower humidity, cloud cover, and rainfall, as well as minimal wind. Following the monsoon rains of June, July, and August, clear skies led to peak radiation levels.

Figure 7 describes the monthly fluctuations in GSR for 2023, 2021, and 2020. Peak GSR values were recorded in May 2023 (20.02 ± 1.52 MJ/m²/day), April 2021 (19.87 ± 0.85 MJ/m²/day), and March 2020 (20.11 ± 0.75 MJ/m²/day), likely due to clear skies following the monsoon rainy season. Conversely, the lowest GSR values occurred in August 2023 (11.87 ± 0.97 MJ/m²/day), January 2021 (11.66 ± 0.59 MJ/m²/day), and September 2020 (8.59 ± 1.08

MJ/m²/day), which can be attributed to cloudy conditions and rainfall. The overall GSR pattern remained consistent across the three years. Error bars, representing standard deviation, indicate the variability of GSR within each month.

Figure 8 gives the seasonal variation of precipitations for 2023, 2021, and 2020. The maximum and minimum rainfall occurs in summer (1096.4 mm) for 2023 and winter (38.43 mm) for the same year over three years respectively. Similarly, figure 9 gives the seasonal variation of average wind speed for 2023, 2021, and 2020. The maximum and minimum average wind speeds occur in spring (1.885 m/s) for 2023 and summer (0.412 m/s) for 2021 among three years respectively.

The intense radiation days of the year are April 25 (28.379 MJ/m²/day), August 6 (32.001 MJ/m²/day), and June 7 (30.049 MJ/m²/day) for the years 2020, 2021, and 2023 respectively. The days with the lowest solar radiation levels were January 17, 2020 (1.548 MJ/m²/day), December 29, 2021 (1.417 MJ/m²/day), and September 23, 2023 (3.552 MJ/m²/day). The maximum temperature days of the year are August 4 (29.5°C), October 12 (28.7°C), and June 8 (28.8°C) for the year 2020, 2021, and 2023 respectively. Similarly, the minimum temperature day of the year is January 6 (0.5°C), January 31 (2°C), and January 20 (2.4°C) for the years 2020, 2021 and 2023 respectively. The maximum rainfall days of the year are September 8 (52.7 mm), July 3 (58.5 mm), and June 19 (71.6 mm) for the years 2020, 2021 and 2023 respectively. The wind speed days of the year are August 29 (2.874 m/s), January 31 (2.262 m/s) and November 7 (3.906 m/s) for the years 2020, 2021 and 2023 respectively.

4.1 Error analysis

Tables 4, 5, and 6 provide a statistical comparison of measured and estimated GSR for 2023, 2021, and 2020, respectively. The correlation and determination coefficients show a moderate relationship between the measured and estimated values in all three years. In 2020 (i.e., $R^2 = 0.64$), 2021 (i.e., $R^2 = 0.64$), and 2023 (i.e., $R^2 = 0.65$), these values are higher for modular CD. Once more, for the CD model in all three years, the values of RMSE, MBE, MPE, and CRM are found less as compared to the other three models. This suggests that among the models, modular CD is better.

Error Analysis

Table 4 Statistical Error of the year 2023 for Taplejung

Model	MBE (MJ/m²/day)	RMSE (MJ/m²/day)	MPE (%)	r	CRM (MJ/m²/day)	R^2	ME	CV
BC	0.0300316	3.53	-6.005	0.7887	0.00	0.60	0.6	22.19
CD	0.0769022	3.28	-5.838	0.8161	0.00	0.65	0.65	20.65
DB	0.0376281	3.58	-7.042	0.7792	0.00	0.59	0.58	22.54
DCBB	0.0636384	3.65	-7.540	0.7699	0.00	0.57	0.57	22.98

Table 5 Statistical Error of the year 2021 for Taplejung

Model	MBE (MJ/m²/day)	RMSE (MJ/m²/day)	MPE (%)	r	CRM (MJ/m²/day)	R^2	ME	CV
BC	0.5622	3.23	-9.1261	0.7676	-0.02	0.63	0.62	22.16
CD	-0.1385	3.18	-4.0940	0.7613	-0.02	0.64	0.64	21.80
DB	0.5486	3.29	-10.5986	0.7462	-0.02	0.61	0.61	22.57
DCBB	0.7379	3.60	-12.1293	0.7165	0.00	0.54	0.53	24.71

Table 6 Statistical Error of the year 2020 for Taplejung

Model	MBE ($MJ/m^2/day$)	RMSE ($MJ/m^2/day$)	MPE (%)	r	CRM ($MJ/m^2/day$)	R^2	ME	CV
BC	-0.0394	3.56	-5.974	0.7533	0.00	0.57	0.56	23.72
CD	-0.6824	3.25	-0.458	0.7992	0.02	0.64	0.63	21.67
DB	-0.0540	3.37	-6.500	0.7690	0.00	0.60	0.60	22.50
DCBB	-0.0016	3.47	-7.189	0.7556	0.02	0.58	0.58	23.15

Figures 1, 2, and 3 illustrate the daily fluctuations in measured and estimated global solar radiation (GSR) for four models in 2023, 2021, and 2020, respectively. The close agreement between estimated and measured daily GSR values across multiple models is significant. The model CD has a greater value of R^2 than the other models for three years, indicating better consistency. Once more, out of the three years, 2023 has greater consistency than 2020 and 2021 for all models. The value of R^2 for 2023, 2021, and 2020 is 65%, 64 %, and 64 % for the CD model respectively. This is due to rainfall and local weather conditions.

Figures 4a, 4b, and 4c show the transmitting coefficient for 2023, 2021, and 2020 respectively. Rainfall causes the sky to become clear, which increases transmittance and, ultimately, GSR in 2022. Figures 5a, b, and c illustrate the daily fluctuations in observed, potential, and transmitted radiation, revealing abundant GSR in the study area. Taplejung's low altitude during winter contributes to a smaller solar angle, resulting in decreased radiation but increased atmospheric transparency. Increased rainfall, cloud cover, and wind speeds during June, July, and August contribute to significantly lower GSR levels in summer compared to other seasons. However, this season is really hot. Rainfall will clear the sky. Thus, there is a high radiation flux during the autumn.

In the year 2021, more rainfall (1792.31 mm) than in the years 2020 (1660.57 mm) and 2023 (1650.82 mm). The combination of higher temperatures and rainfall during summer leads to reduced GSR. Overall, GSR increases steadily from June to August before decreasing gradually until December. However, GSR's trend changes because of its dependence on precipitation and temperature. Because of the rain and cloudy sky in June, July, and August, GSR is lower. The GSR has a direct relationship with temperature and a negative relationship with precipitation.

The mountainous Simikot region, situated at a higher altitude, receives less GSR compared to the mid-hill location of Jumla. GSR values for Simikot were 6648 $MJ/m^2/day$ in 2013 and 7309 $MJ/m^2/day$ in 2011. The BC model is more suitable for estimating GSR in Jumla than in Simikot. While Simikot experiences higher GSR during spring and autumn, Jumla's peak GSR occurs in the spring. The local weather and variations in altitude are the causes of this effect (Chhetri and Gurung 2017).

Although Simikot is at a higher altitude, Jumla receives more sunlight. This is likely due to several factors, such as clearer skies and less cloud cover in Jumla, which allow more direct sunlight to reach the ground. Seasonal changes, especially during spring when the sun is directly overhead, can also contribute to Jumla's higher solar radiation. The specific locations and measurement methods used could also play a role in the recorded data, emphasizing that solar radiation patterns can vary significantly between different regions.

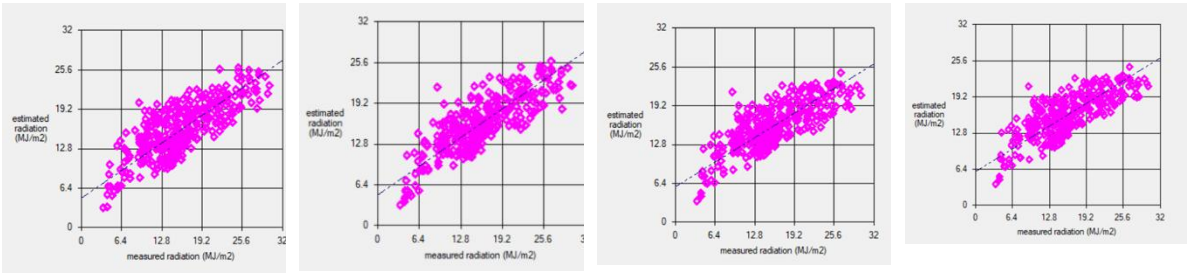

BC 2023 **CD 2023** **DB 2023** **DCBB 2023**

Fig. 1 Linear relationship analysis of measured and estimated GSR data for Taplejung in 2023.

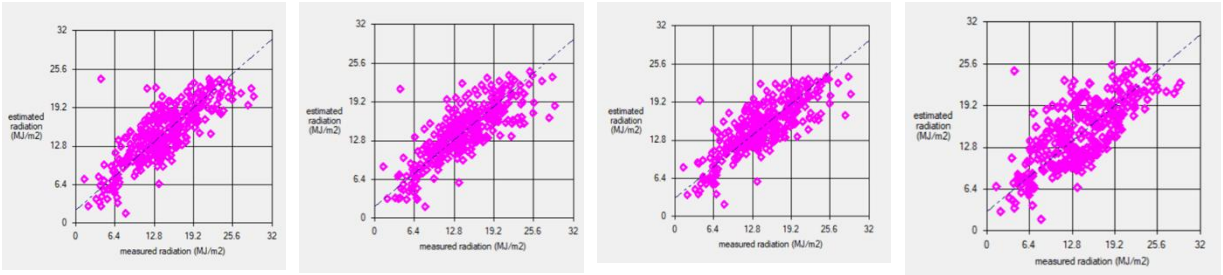

BC 2021 **CD 2021** **DB 2021** **DCBB 2021**

Fig. 2 Linear relationship analysis of measured and estimated GSR data for Taplejung in 2021

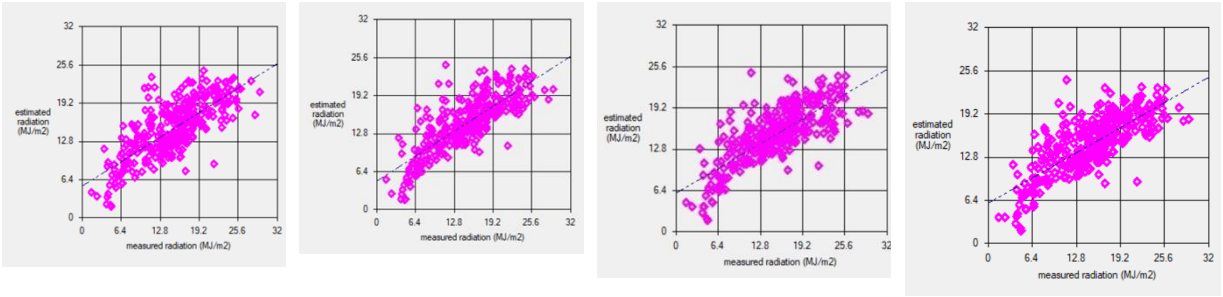

BC 2020 **CD 2020** **DB 2020** **DCBB 2020**

Fig. 3 Linear relationship analysis of measured and estimated GSR data for Taplejung in 2020

.

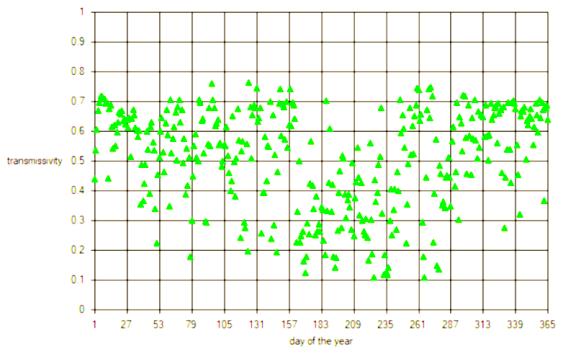

4 a. Daily Transmissivity coefficient 2023

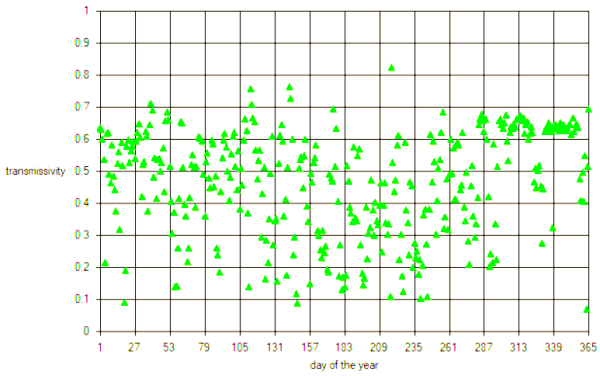

4 b. Daily Transmissivity coefficient 2021

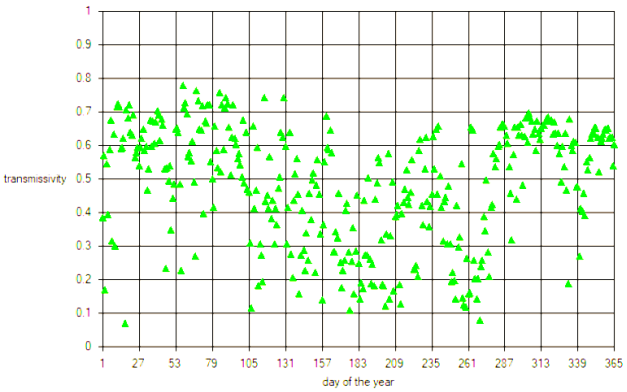

4 c. Daily Transmissivity coefficient 2020

Fig. 4 Fluctuations in the daily transmissivity coefficient for Taplejung during 2023, 2021, and 2020

.

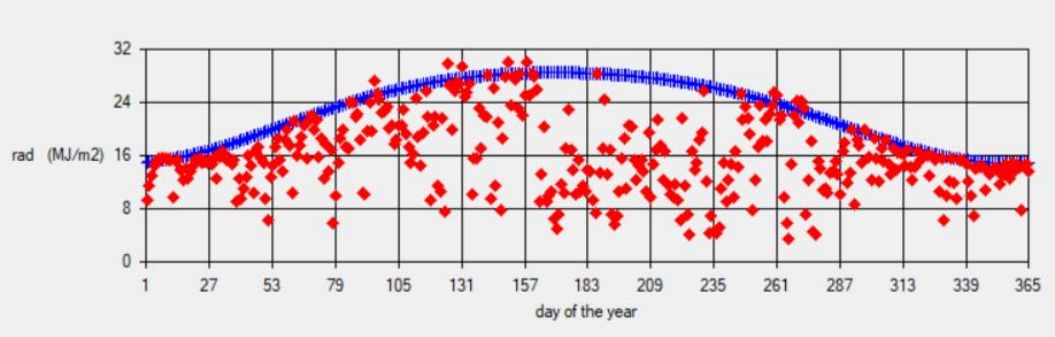

a. Daily fluctuations in GSR at Taplejung for 2023

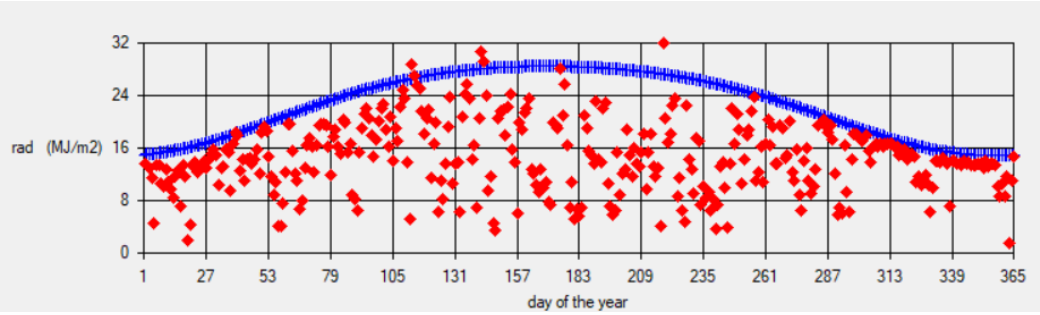

b. **Daily fluctuations in GSR at Taplejung for 2021**

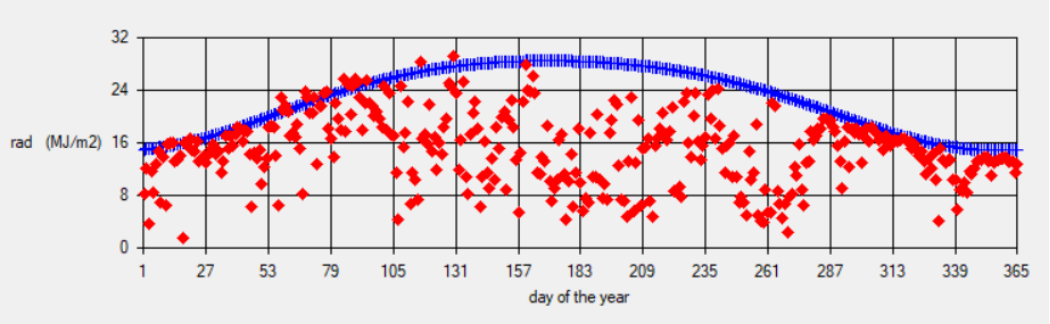

c. Daily fluctuations in GSR at Taplejung for 2020

Fig. 5 Daily fluctuations in GSR at Taplejung for 2023, 2021, and 2020

...

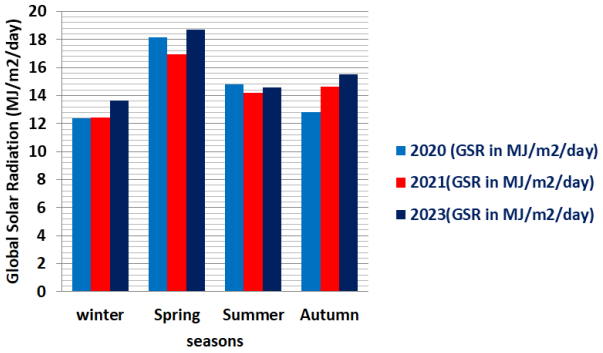

Fig. 6 Seasonal Fluctuation of GSR

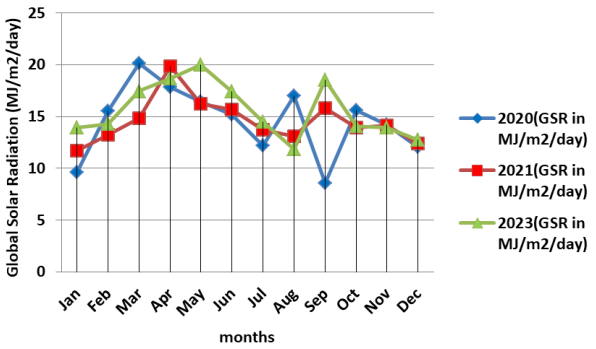

Fig. 7 Monthly Fluctuation of GSR

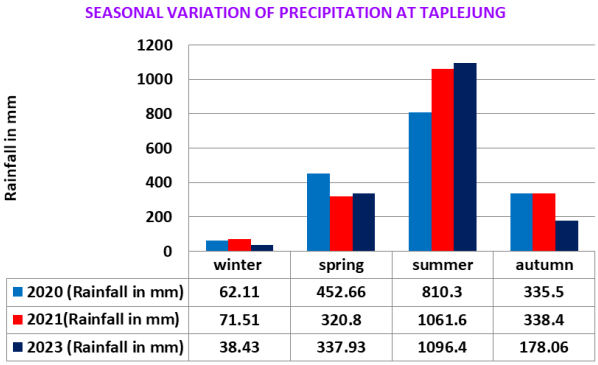

Fig. 8 Seasonal Fluctuation of Precipitation

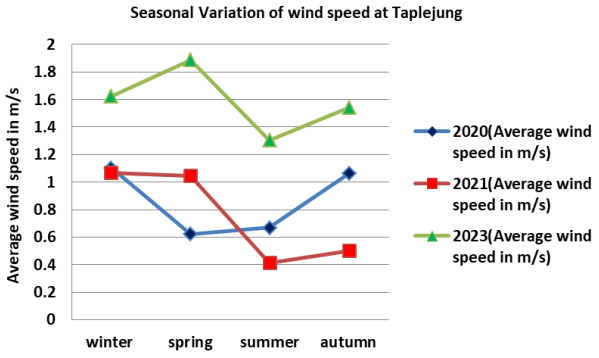

Fig. 9 Seasonal Fluctuation of average wind speed

5 CONCLUSIONS

The average daily annual GSR in Taplejung was determined to be 15.0 ± 0.31 MJ/m²/day, 14.6 ± 0.28 MJ/m²/day, and 15.9 ± 0.31 MJ/m²/day for 2020, 2021, and 2023, respectively. These values indicate significant solar energy potential, making it suitable for developing both grid-connected and off-grid power plants in the region, which currently faces energy shortages. Factors such as temperature, humidity, rainfall, wind speed, and sunshine duration influence the variability of solar radiation intensity over time and location.

Because of ground albedo, radiation rises after monsoon on clear sky days. Therefore, topography and local meteorological conditions are important factors in estimating GSR in many locations. In summary, Taplejung has solar insolation of 4.42 ± 0.09 kWh/m²/day, which offers significant potential for rapid solar energy development. The combination of low air pollution, precipitation, cloud cover, reduced humidity, and south-facing mountain topography creates ideal conditions for high solar insolation.

RadEst 3.0 is used to test four models in our research analysis. This high-mountain region is best suited for using the CD model among the four models since it has the highest coefficient of determination and fewer errors than the other three. In conclusion, the empirical coefficients derived from the CD model can be effectively utilized to predict solar radiation and energy levels in regions of Nepal with similar geographical characteristics.

Acknowledgement

The authors express sincere thanks to the FAOSDRN Agrometeorology Group in Rome and ISCI-Crop Science in Bologna for providing free access to the RadEst 3.0 software and documentation for educational purposes. They also acknowledge the Department of Hydrology and Meteorology (DHM) in Nepal for supplying meteorological data. Finally, the authors extend their gratitude to all who contributed to the study.

Funding: This research was conducted independently without external financial support.

Declarations: The authors declare no conflicts of interest.

REFERENCES

[1] Akpootu, D. O., Alaiyemola, S. R., Abdulsalam, M. K., Bello, G., Umar, M., Aruna, S., ... & Badmus, T. O. (2023). Sunshine and temperature-based models for estimating global solar radiation in Maiduguri, Nigeria. *Saudi Journal of Engineering and Technology*, *8*(5), 82-90.

[2] Allen RG (1997) Self-calibrating method for estimating solar radiation from air temperature. J Hydrol Eng 2(2):56–67

[3] An, Y., Chen, T., Shi, L., Heng, C. K., & Fan, J. (2023). Solar energy potential using GIS-based urban residential environmental data: A case study of Shenzhen, China. Sustainable Cities and Society, 93, 104547.

[4] An, Y., Chen, T., Shi, L., Heng, C. K., & Fan, J. (2023). Solar energy potential using GIS-based urban residential environmental data: A case study of Shenzhen, China. *Sustainable Cities and Society*, *93*, 104547.

[5] Angstrom A (1924) Solar and terrestrial radiation. Report to the International Commission for Solar Research on actinometric investigations of solar and atmospheric radiation. Quarterly J Royal Meteorol Soc 50(210):121–126

[6] Annandale J, Jovanovic N, Benade N, Allen R (2002) Software for missing data error analysis of penman-monteith reference evapotranspiration. Irrig Sci 21(2):57–67
[7] Bristow KL, Campbell GS (1984) On the relationship between incoming solar radiation and daily maximum and minimum temperature. Agric for Meteorol 31(2):159–166
[8] Chhetri BRK, Gurung S (2017) Estimation of total solar radiation using Radest 3.00 software at Jumla, Nepal. Int J Syst Assur Eng Manag 8(2):1527–1533
[9] Dhakal S, Gautam Y, Bhattarai A (2020) Evaluation of temperature-based empirical models and machine learning techniques to estimate daily global solar radiation at Biratnagar Airport Nepal. Adv Meteorol 2020:1–11
[10] Donatelli M, Bellocchi G, (2001) Estimate of daily global solar radiation: new developments in the software radest3.00. In: Proceedings of the 2nd international symposium modeling cropping systems, Inst. for Biometeorology CNR, Florence, Italy, 213–214
[11] Donatelli M, Bellocchi G, Fontana F (2003) Radest3.00: software to estimate daily radiation data from commonly available meteorological variables. Eur J Agron 18(3–4):363–367
[12] Donatelli, M. Campbell, G.S. 1998, *"A simple model to estimate global solar radiation"*, Proceedings of the 3rd Congress of the Europe Society for Agronomy, Nitra, Slovakia, II, pp. 133–134.
[13] Golden Software/Surfer. Surfer 13. [Online; accessed 26-March- 2019]
[14] González-Plaza, E., García, D., & Prieto, J. I. (2024). Monthly Global Solar Radiation Model Based on Artificial Neural Network, Temperature Data and Geographical and Topographical Parameters: A Case Study in Spain. *Sustainability*, *16*(3), 1293.
[15] Goodin DG, Hutchinson J, Vanderlip RL, Knapp M (1999) Estimating solar irradiance for crop modeling using daily air temperature data. Agron J 91(5):845–851
[16] Hassan GE, Youssef ME, Mohamed ZE, Ali MA, Hanafy AA (2016) New temperature-based models for predicting global solar radiation. Appl Energy 179:437–450
[17] Iqbal M (1983) An introduction to solar radiation. Academic Press, New York, NY
[18] Joshi U, Karki IB, Chapagain NP, Poudyal KN (2021) Prediction of daily global solar radiation using different empirical models based on meteorological parameters at Trans Himalaya Region. Nepal BIBECHANA 18(1):159–169
[19] Joshi U, Poudyal KN, Karki IB, Chapagain NP (2020) Evaluation of global solar radiation using sunshine hour, temperature and relative humidity at low land region of Nepal. J Nepal Phys Soc 6(1):16–24
[20] Joshi, U., Chapagain, N. P., Karki, I. B., Shrestha, P. M., & Poudyal, K. N. (2022). Estimation of daily solar radiation flux at Western Highland, Simikot, Nepal using RadEst 3.0 software. *International Journal of System Assurance Engineering and Management*, *13*(1), 318-327.
[21] Kudish A, Wolf D, Machlav Y (1983) Solar radiation data for beer Sheva. Israel Solar Energy 30(1):33–37
[22] Lamsal H (2019) Nea to connect all households with electricity by 2022. Republica
[23] Li H, Cao F, Wang X, Ma W (2014) A temperature-based model for estimating monthly average daily global solar radiation in China. Sci World J 2014:1–9
[24] Nage GD (2018) Estimation of monthly average daily solar radiation from meteorological parameters: sunshine hours and measured temperature in Tepi, Ethiopia. Int J Energy Environ Sci 3(1):19–26
[25] Narejo, K. A., Rehman, S. U., Tariq, I., Zahid, M. M., Sadiq, N., Khan, M. M., & Uddin, Z. (2024). MEP modelled new equations for ASHRAE constant to estimate solar radiation. *Indian Journal of Physics*, 1-5.
[26] Olomiyesan B, Oyedum O, Ugwuoke P, Abolarin M (2017) Evaluation of some global solar radiation models in selected locations in northwest, Nigeria. Open Access J Photo Energy 1(1):1–6
[27] Poudyal K N (2015) Estimation of global solar radiation potential in Nepal. Ph D Thesis, IOE, Tribhuvan University
[28] Poudyal KN, Bhattarai BK, Sapkota B, Kjeldstad B (2012) Estimation of the daily global solar radiation using RadEst 3.00 software-a case study at low land plain region of Nepal. J Nepal Chem Soc 29:48–57
[29] Poudyal KN, Bhattarai BK, Sapkota B, Kjeldstad B, Daponte P (2013) Estimation of the daily global solar radiation; Nepal experience. Measurement 46(6):1807–1817
[30] Radest 3.00 version. [Online; accessed 26-March-2019]
[31] Radiation in central European lowlands is estimated by various empirical formulae. A` gric For Meteorol 131(1–2):54–76
[32] Rajbanshi, B. K., Singh, R. G., KC, B. R., & Poudel, K. N. (2024). Comparative analysis of different models within

RadEst 3.0 for solar radiation estimation at Dhankutta, Nepal. *Journal of Nepal Physical Society, 10*(1), 70–76. (A)

[33] Rajbanshi, B. K., Singh, R. G., Khatiwada, K., Thapa, A., & KC, B. R. (2024). Comparative analysis of empirical models for estimating global solar radiation in Biratnagar, Nepal: A case study using RadEst 3.0. *Nanotechnology Perceptions, 20*(S16). (B)

[34] Research Centre for Industrial Crops Agriculture Research Council.

[35] Romero-Ramos, J. A., Gil, J. D., Cardemil, J. M., Escobar, R. A., Arias, I., & Pérez-García, M. (2023). A GIS-AHP approach for determining the potential of solar energy to meet the thermal demand in southeastern Spain productive enclaves. *Renewable and Sustainable Energy Reviews*, *176*, 113205.

[36] Shrestha JN, Bajracharya T, Shakya S, Giri B (2003) Renewable energy in Nepal-progress at a glance from 1998 to 2003. In: proceedings of the international conference on renewable energy technology for rural development (RETRUD-03), pages 12–14

[37] Team, GEAW et al. (2012). Global energy assessment. Cambridge Books

[38] WECS, Energy Synopsis Report, 2023, Government of Nepal